ISSN 1023-1935, Russian Journal of Electrochemistry, 2019, Vol. 55, No. 7, pp. 643–650. © Pleiades Publishing, Ltd., 2019.
Published in Russian in Elektrokhimiya, 2019, Vol. 55, No. 7, pp. 832–840.

Investigation of Proton Diffusion Coefficient for PbO_2 Prepared from Intermediate Oxides

L. Rahmani[a], R. Fitas[a], A. Messai[b, *], and A. I. Ayesh[c, **]

[a] *Laboratoire de Croissance et Caractérisation de Nouveaux Semi-conducteurs, Université Ferhat Abbas, Sétif-1, 19000 Algeria*
[b] *Laboratoire d'Ingénierie et Sciences des Matériaux Avancés (ISMA), Institut des Sciences et Technologie, Abbès Laghrour University, Khenchela, 40000 Algeria*
[c] *Department of Mathematics, Statistics and Physics, Qatar University, Doha, Qatar*
**e-mail: Messamel1@gmail.com*
***e-mail: ayesh@qu.edu.qa*

Received March 29, 2018; revised July 28, 2018; accepted August 27, 2018

Abstract—Lead dioxide was extracted from used batteries, and used to synthesize the following intermediate oxides by heating at different temperatures: $Pb_{12}O_{19}$, $Pb_{12}O_{17}$, and Pb_3O_4. Each of the prepared intermediate oxide was subject to sulfuric acid with 1.28 $g.cm^{-3}$. X-ray diffraction (XRD) results showed that the sample prepared from $Pb_{12}O_{19}$ only had a pattern similar to that of the starting PbO_2 with α-PbO_2 and β-PbO_2 phases. The measurements of H^+ proton diffusion coefficient (D_{H+}) of the different samples showed that the sample prepared from $Pb_{12}O_{19}$ had better electrochemical performances than the starting PbO_2. This kinetics reflects the proton insertion mechanism in PbO_2, i.e. the sample prepared from $Pb_{12}O_{19}$ has a large amount of structural water in OH^- hydroxyl form. This amount contributes more in the PbO_2 reduction mechanism. In addition, the D_{H+} value of the sample prepared from $Pb_{12}O_{19}$ is significantly higher than that of starting PbO_2, which confirms this hypothesis. X-ray diffraction analysis, thermogravimetric and differential thermogravimetry analysis, and cyclic voltammetry reduction at different scanning rates were used to investigate the samples. This work contributes to environment preservation by recycling of used lead dioxide and reduction of the hazard of its disposal on water.

Keywords: lead-acid batteries, sulfuric acid, α-PbO_2 and β-PbO_2, intermediate lead oxides, lead dioxide, thermal analysis, structural water

DOI: 10.1134/S1023193519070103

INTRODUCTION

Lead dioxide (PbO_2) is a key element of the positive plates of the lead-acid batteries. The texture and structure of lead dioxide have great influence on the electrochemical and electrical performance of the battery. Herein, two phases of PbO_2 are present on the positive plate of a battery: α-PbO_2 which crystallizes in an orthorhombic structure, and β-PbO_2 which crystallizes in a tetragonal structure. In addition, the α and β phases of PbO_2 do not correspond to the stoichiometric chemical formula (PbO_2) [1, 2]. Therefore, the presence of either of these varieties of dioxides in different proportions influence the electrochemical behavior of a positive plate. The proper functioning of lead accumulator is linked to the ratio α-PbO_2 to β-PbO_2 existing on the plate.

Numerous authors have studied the crystallographic structures of α-PbO_2 and β-PbO_2 by both X-ray diffraction (XRD) [3–5], and by neutron diffraction [6, 7]. Different studies [8–10] showed the existence of protonated species within the PbO_2 lattice, but they were unable to locate them on structural positions. In our previous work [1, 2, 11–13], we found that the electrochemical activity of PbO_2, which constitutes the active mass of the positive plate, depends on the surface of structural water. Therefore, the shelf life of a lead-acid battery depends on the nature and quantity of these hydrogen species. The active mass is a gel–crystal system (hydrogen species) that conducts electricity by electrons and protons in hydrated areas of the gel zone [14–17]. Using X-ray photoelectron spectroscopy (XPS) technique, Pavlov [14, 18] found that greater than 30% of the surface for PbO_2 is hydrated.

Lead dioxides can be prepared in the lab either by a chemical route, or by electrochemical route. It is known that PbO_2 prepared by chemical route is inactive, while that prepared by electrochemical process is very active [11, 19–22]. The electrochemical activity

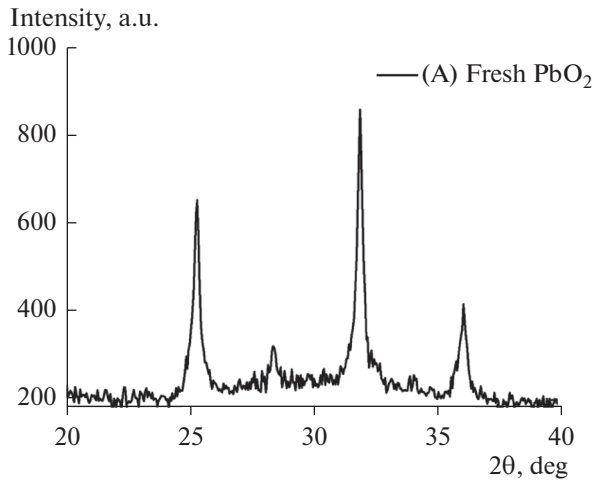

Fig. 1. XRD patterns of fresh PbO_2 retrieved from a used battery (sample A).

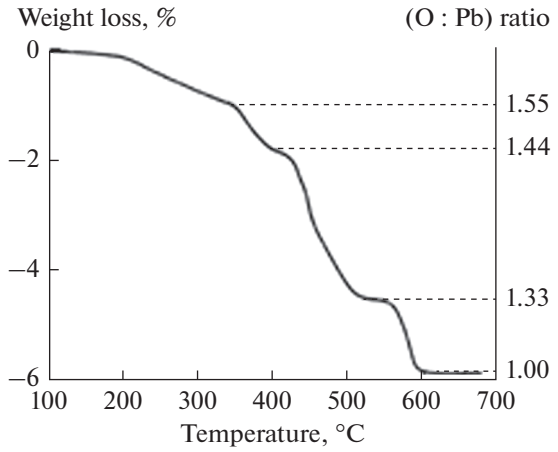

Fig. 2. Thermogravimetric curve of fresh PbO_2 (sample A).

of PbO_2 is directly related to the existence of protonated species in the gel zones. This characteristic has led many authors to propose different formalisms. For example, a model was proposed by J.P. Pohl et al. [19, 23] suggested the composition of $PbO_{2-\delta} \cdot mH_2O$, where δ denotes oxygen deficiency, and *m* denotes the quantity of water. Rüetschi [24, 25] proposed another model of lead gap, considering that all water is in the form of OH^- associated with gaps of Pb^{4+} or Pb^{2+} ions. Based on this model, they attributed the following chemical formula to PbO_2: $Pb^{4+}_{1-y}Pb^{2+}_{y}O^{2-}_{2-2y}OH^{-}_{2y}$. Here, *y* donates the fraction of Pb^{2+} substituted by OH^- ions.

The source of the electrochemical activity was mainly connected to the existence of hydrogen species. Several authors [26, 27] showed by nuclear magnetic resonance (NMR), as well as by inelastic [28, 29] and quasi-elastic scattering of neutron (NQES) studies [30, 31] the existence of two configurations, at least, for the protons in the electrochemically active PbO_2, and a single configuration of chemically prepared inactive PbO_2. Here, hydrogen-combined compounds were recognized in PbO_2 as H_2O and OH^- groups.

The aim of this study is to compare the values of diffusion coefficient of proton (D_{H+}) in PbO_2 recovered from intermediate oxides PbO_x ($1.33 < x < 2$) after exposure to sulfuric acid solution. The new oxides result in spontaneous chemical reactions led to the formation of new phases of PbO_2, thus, showing the instability of these oxides in sulfuric acid. The new positive active masses (PAMs) were characterized by XRD technique, and thermal analyses. In addition, a voltamperometry technique was utilized to determine the H^+ diffusion coefficient of the proton in PbO_2.

EXPERIMENTAL

Sample Preparation

Fresh PbO_2 was taken from industrial positive plates of used lead-acid batteries. PbO_2 was then washed with water and then dried at 105°C for 24 h. Extracted PbO_2 powder, was hot washed with saturated solution of ammonium acetate optionally to eliminate lead sulfates untrained, then dried in open air overnight. This sample was named as sample A. The material was crushed and sieved using a sieve of 50 microns. The sample was identified by XRD analysis as shown in Fig. 1. The XRD measurements were performed using the Debye–Scherrer method [32]. We note that the experimental peaks obtained for the sample are indexed perfectly with the American metals testing system (ASTM) cards nos. 11-549 and 25-447 of α-PbO_2 and β-PbO_2, respectively, indicating that the prepared sample is pure.

The sample was tested by thermal gravimetric analysis (TGA), and followed by differential thermal analysis (DTA) using thermal balance analyzers type (SETARAM model RT 3000 and PRT 540). Assays were performed at temperatures ranging from ambient to 700°C with a heating rate of 10°C/min.

Examination of TGA curves in Fig. 2 shows three distinct temperature zones. The first zone between 20 and 230°C, corresponds to a decrease in weight from water. The second zone is between 230 and 450°C, a sharper decrease in weight corresponds to oxygen loss that give rise to the appearance of successive intermediate oxides. This explains the decrease of oxygen ratio to lead depending on the heating temperature. The O : Pb ratios are shown on the minor *y*-axis of the figure. The third zone is assigned to the decomposition of oxides result in the appearance of Pb_3O_4 at around 480°C. Between the first and the second transitions, the

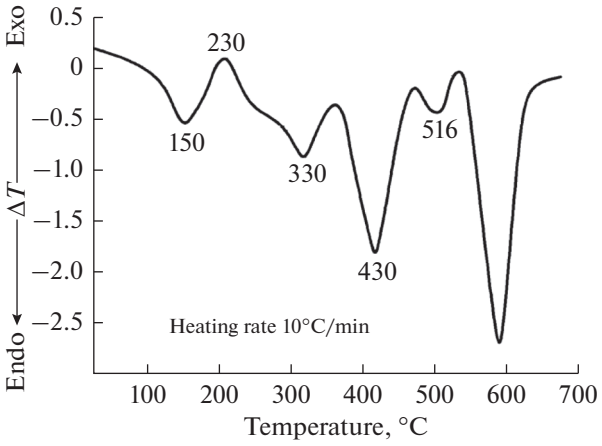

Fig. 3. DTA curve of fresh PbO_2 (sample A). The temperatures quoted in red font are the transition temperatures of the intermediate oxides.

formation of intermediate oxides PbO_x ($1.33 \le x \le 2$) occurs.

The DTA curve in Fig. 3 shows several endothermic and exothermic peaks: (i) a broad endothermic peak and flattened linked from surface water, (ii) an exothermic peak from water structure (this peak is preceded by a slight shoulder); and (iii) three peaks of endothermic transition in the temperature range between 300 and 550°C correspond to the formation of $Pb_{12}O_{19}$, $Pb_{12}O_{17}$, and Pb_3O_4. The transition temperatures match well with the TGA results in Fig. 2.

Fresh PbO_2 (sample A) was taken from commercial positive plates of used lead acid batteries. Intermediate oxides were prepared by heating fresh samples of PbO_2 up to 8 h at 330, 430, and 516°C (these temperatures were taken from the DTA curve of Fig. 3) to produce $Pb_{12}O_{19}$, $Pb_{12}O_{17}$, and Pb_3O_4 oxides, respectively, according to the following equations:

$$12PbO_2 \xrightarrow{\text{Heating at } 300^\circ\text{C}} Pb_{12}O_{19} + \left(\frac{5}{2}\right)O_2,$$

$$12PbO_2 \xrightarrow{\text{Heating at } 430^\circ\text{C}} Pb_{12}O_{17} + \left(\frac{7}{2}\right)O_2,$$

$$3PbO_2 \xrightarrow{\text{Heating at } 516^\circ\text{C}} Pb_3O_4 + O_2.$$

The phase composition of the different samples was determined by XRD analysis as revealed in Fig. 4a. Figure also demonstrates that heating the sample up to 230°C causes loss of water with maintaining the initial structure and reduces line intensities. The compositions of the various samples are summarized in Table 1. The table reveals that heating to 8 h is needed for complete transformation into $Pb_{12}O_{19}$, $Pb_{12}O_{17}$, and Pb_3O_4 oxides.

The intermediate oxides were mixed with under stirring for 1 h. PbO_2 powders recovered from the reaction of the intermediate oxides with sulfuric acid with 1.28 g cm^{-3} were rinsed with a solution of boiling saturated ammonium acetate to remove any $PbSO_4$, filtered, washed with distilled water, and then dried overnight at 105°C. These samples were named as: (A) for fresh PbO_2; while (B), (C), and (D) belong to the samples result from the reaction with sulfuric acid of $Pb_{12}O_{19}$, $Pb_{12}O_{17}$, and Pb_3O_4, respectively. The reactions with sulfuric acid are described below, and the samples were identified by XRD as shown in Fig. 4b.

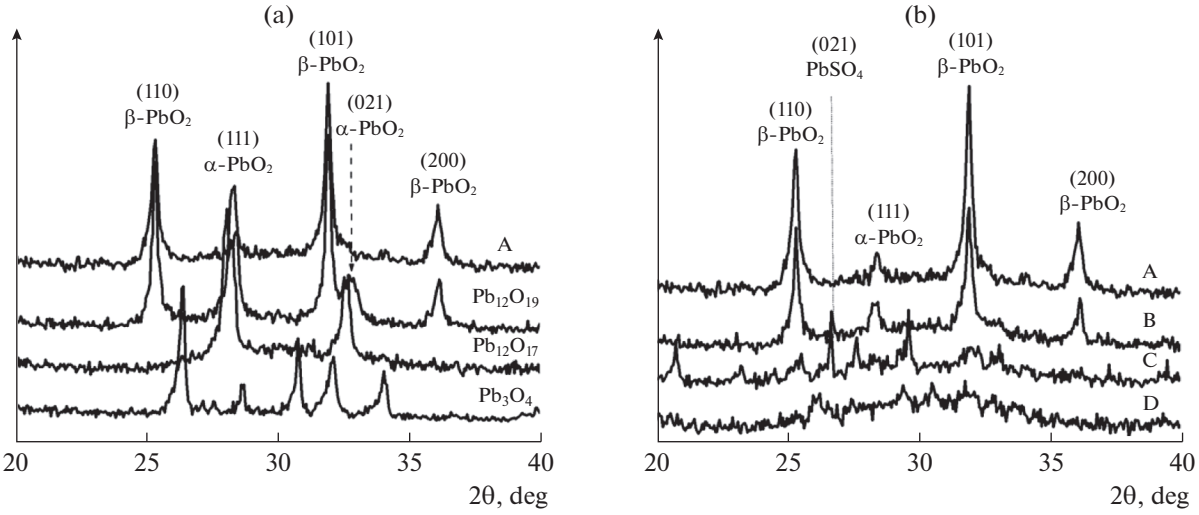

Fig. 4. (a) XRD patterns of fresh PbO_2 (sample A) and its intermediate oxides ($Pb_{12}O_{19}$, $Pb_{12}O_{17}$, and Pb_3O_4). (b) XRD patterns of fresh PbO_2, (sample A) and the samples synthesized from intermediate oxides after reaction with sulfuric acid (B, C, and D).

Table 1. The compositions of the various lead oxides result from heating PbO_2 at different temperatures for different periods

T, °C	Heating time		
	4 hours	6 hours	8 hours
330	55.14% $Pb_{12}O_{19}$; 44.86% α-PbO_2	74.2% $Pb_{12}O_{19}$; 25.8% α-PbO_2	99.11% $Pb_{12}O_{19}$; 0.89% α-PbO_2
430	64.66% $Pb_{12}O_{17}$; 35.34% Pb_3O_4	80% $Pb_{12}O_{17}$; 20% Pb_3O_4	100% $Pb_{12}O_{17}$
516	71.88% Pb_3O_4; 28.12% PbO	94.92% Pb_3O_4; 5.08% PbO	100% Pb_3O_4

$$a_1Pb_{12}O_{19} + b_1H_2SO_4 \rightarrow \underbrace{c_1PbO_2(\text{new phase})}_{\text{Sample B}} + \underbrace{d_1PbSO_4}_{\text{Treated with hot ammonium acetate}} + e_1H_2O,$$

$$a_2Pb_{12}O_{17} + b_2H_2SO_4 \rightarrow \underbrace{c_2PbO_2(\text{new phase})}_{\text{Sample C}} + \underbrace{d_2PbSO_4}_{\text{Treated with hot ammonium acetate}} + e_2H_2O,$$

$$a_3Pb_3O_4 + b_3H_2SO_4 \rightarrow \underbrace{c_3PbO_2(\text{new phase})}_{\text{Sample D}} + \underbrace{d_3PbSO_4}_{\text{Treated with hot ammonium acetate}} + e_3H_2O.$$

Electrochemical Investigations

Electrochemical tests were applied in a conventional three-electrode cell. PbO_2 served as the working electrode, while the counter electrode is a large sheet of platinum foil. The potential was measured against an Hg/Hg_2SO_4 calomel electrode. The electrolyte was a solution of sulfuric acid with 1.28 g cm^{-3}. To assess the diffusion coefficient value of proton within PbO_2 groups resulting from the intermediate oxides, reduction voltamperometric technique was used at various scanning rates. Potentiodynamic scanning cycles were ranged between 500 and 1400 mV reference to the Hg/Hg_2SO_4 calomel electrode at various scanning rates (5, 25, 50, and 100 mV/s).

RESULTS AND DISCUSSION

Figure 4a presents the XRD patterns of fresh PbO_2 (sample A) and its intermediate oxides produced by heating ($Pb_{12}O_{19}$, $Pb_{12}O_{17}$, and Pb_3O_4). Fresh lead dioxide is indexed as β-PbO_2 with a percentage of α-phase. In addition, we note on one hand that $Pb_{12}O_{19}$ conserves almost the same structure as that of the fresh PbO_2 and exhibits a pattern similar to that of β-PbO_2 with an increase in the content of α-PbO_2. On the other hand, the intermediate oxides namely $Pb_{12}O_{17}$ and Pb_3O_4 respectively present patterns that are totally different from that of the fresh PbO_2. This means that the heating temperature is important in the process of preparation of intermediate oxides. In light of the above findings, we propose the following mechanism of thermal degradation of the PbO_2 mass following equation:

$$PbO_2 \rightarrow Pb_{12}O_{19} \rightarrow Pb_{12}O_{17} \rightarrow Pb_3O_4.$$

Figure 4b presents the XRD patterns of the PbO_2 powders synthesized from the reaction of the intermediate oxides with sulfuric acid compared to that of fresh lead dioxide. We can deduce that sample B (PbO_2 prepared from $Pb_{12}O_{19}$) exhibits a pattern similar to that of sample A (fresh PbO_2). The figure reveals that sample B exhibits a pattern similar to that of sample A with the peaks of both α and β phases of PbO_2. In addition, a new peak is observed at $2\theta = 26.8°$ which is probably due to the presence of $PbSO_4$ crystals. The average crystal size for samples A and B was determined from the full width at the half maximum (FWHM) for the [110] diffraction line using Scherrer's equation. Sample B yields a crystal size of 14.85 nm while sample A size is 22.30 nm. Consequently, sample B is more amorphous than the fresh PbO_2. The other samples (C and D) show patterns that are different from the reference sample. This can be explained by the fact that these oxides were prepared, respectively, from $Pb_{12}O_{17}$ and Pb_3O_4 that are synthesized from fresh PbO_2 at high temperature. These samples already lost a certain amount of their oxygen in addition to structural water which is difficult to recover it from the aqueous solution when treated with H_2SO_4.

Figure 5 represents the voltammograms related to the different samples for scanning rates ranging between 5 to 100 mV/s. The figures reveal that: (i) the

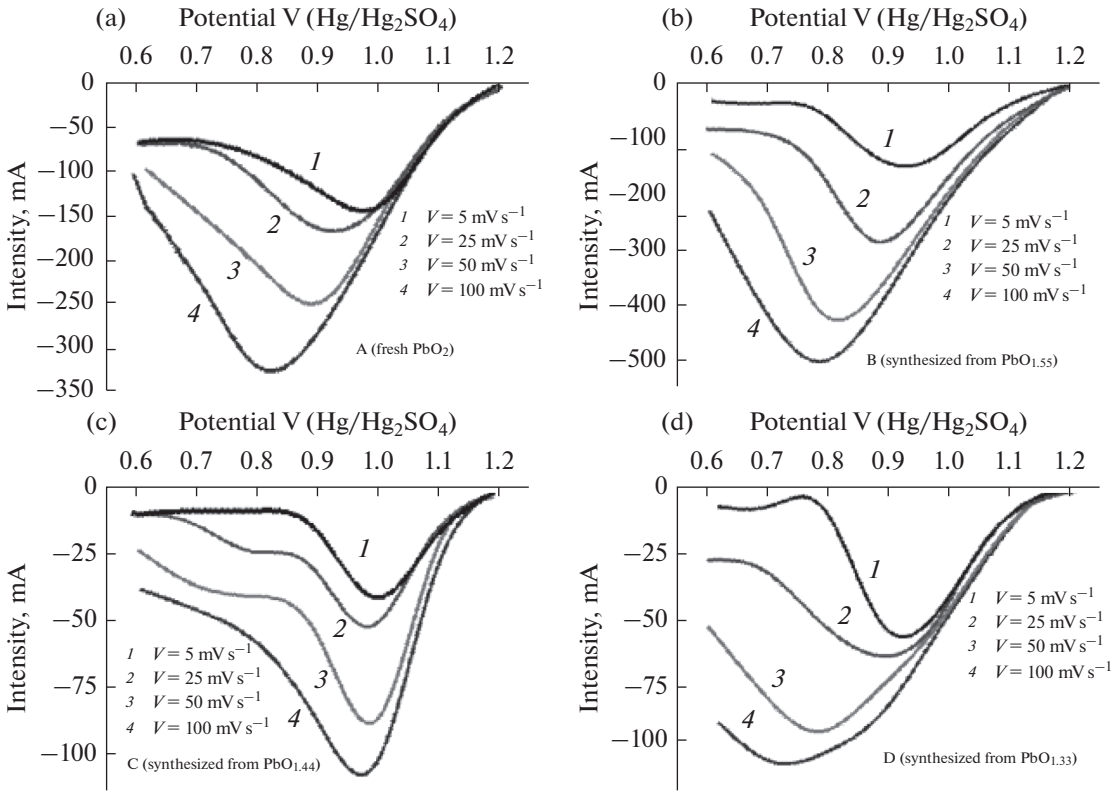

Fig. 5. (a) Voltammograms at various scanning rates for (a) A sample (fresh PbO_2), (b) B sample produced from produce $Pb_{12}O_{19}$ oxide, (c) C sample produce from $Pb_{12}O_{17}$ oxide, and (d) D sample produced from Pb_3O_4 oxide.

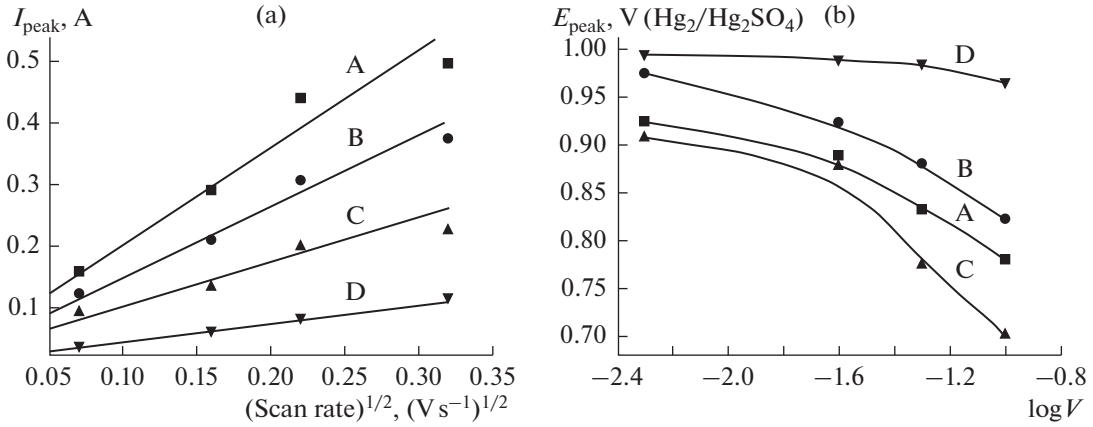

Fig. 6. (a) Dependence of I_{peak} on V^2 for samples A, B, C, and D. (b) Dependence of E_{peak} on log(V) for samples A, B, C, and D.

cathodic peak strength increases with the increasing scan rate, and (ii) cathodic peak potentials are shifted negatively towards less positive potential values.

Electronic Mechanisms

Investigation of the various voltamogram peaks drawn at various scan rates give information about the nature of the limiting step in an electrochemical process. Here: (i) the variations of current intensity of the peak (I_{peak}) is with the square root of scan rate ($I_{peak} = f(V^{1/2})$), and ii) the variations of tension peak (E_{peak}) is with the logarithm of the scan rate ($E_{peak} = f(\log(V))$).

Figure 6a presents the variation of I_{peak} with $V^{1/2}$ for the different samples. The dependence is a linear increase of I_{peak} with $V^{1/2}$. Variation of E_{peak} with log(V) for the different samples is presented in Fig. 6b. The

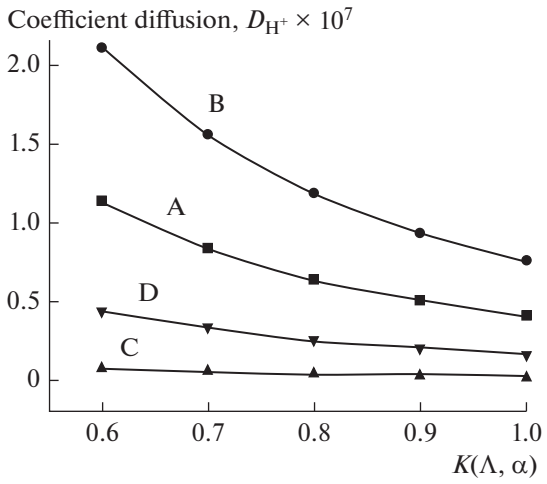

Fig. 7. Variation of the diffusion coefficient D_{H^+} as a function of the constant $K(\Lambda, \alpha)$ for samples A, B, C, and D.

figure shows that the curves are concave down. This process is in agreement with the case of an electrochemical semi-rapid or quasi-reversible process where $I_{peak} = f(V^{1/2})$ is linear, here, the peak current is a diffusion current [33].

Determination of Diffusion Coefficient

For a process controlled by diffusion, the general expression of peak current in case of a quasi-reversible system is given by the following equation [33]:

$$I_{peak} = \left[\left(2.69 \times 10^5\right) n^{3/2} A D_{H^+}^{1/2} C_{H^+} K(\Lambda, \alpha)\right] V^{1/2}. \quad (1)$$

Here, I_{peak} has a linear dependence on $V^{1/2}$ with a slope of $(2.69 \times 10^5) n^{3/2} A D_H{}^{+1/2} C_H{}^{+} K(\Lambda, \alpha)$. Where n is the number of exchanged electrons, A is the electrode surface expressed in cm^2, and C_{H+} is H^+ ion concentration (mol/l). The constant $K(\Lambda, \alpha)$ depends mainly on a dimensional parameter Λ, and the cathodic charge transfer coefficient α. This constant was introduced by Matsuda and Ayabe [33], and its value varies from 0.6 and 1.0. Table 2 summarizes the equations of I_{peak} lines with $V^{1/2}$ and the corresponding slope values.

Figure 7 reveals the dependence of diffusion coefficient of H^+ as a function of the constant $K(\Lambda, \alpha)$ for samples A, B, C, and D. Figure demonstrates: (i) the diffusion coefficient of H^+ value decreases when $K(\Lambda, \alpha)$ increases, particularly for samples A and B; (ii) the diffusion coefficient of H^+ value is almost independent of $K(\Lambda, \alpha)$ for sample C; and (iii) for the low values of $K(\Lambda, \alpha)$, a gap in D_{H^+} values is observed for samples A, B and C. This gap decreases gradually with increasing $K(\Lambda, \alpha)$ value. Table 3 demonstrates the values of the diffusion coefficient of H^+ as a function of the constant $K(\Lambda, \alpha)$. It should be noted here that the values estimated from Table 3 are similar to those found by Münzberg and Pohl [34] (they estimated the diffusion coefficient of H^+ of PbO_2 by an electrochemical method for different pH and Pb^{2+} concentrations, and the values were found to vary between 0.4 and 4.9×10^{-7} $cm^2\,s^{-1}$). It should be noted that the values of D_{H^+} for both α- and β-PbO_2 were also reported as 9.6×10^{-10} and 2.2×10^{-9}, respectively, in reference [35], and 5×10^{-13} and 10^{-14} $cm^2\,s^{-1}$, respectively, in [35]. The table reveals that sample B exhibit the highest values of D_{H^+} compared with other samples regardless of the value of $K(\Lambda, \alpha)$. For example, for $K(\Lambda, \alpha) = 0.6$, D_{H^+} of sample B is higher than that of sample A by 0.98×10^{-7} $cm^2\,s^{-1}$, which represents an increase of around 86%. This can be explained by the rate of presence of water physisorbed as OH^- groups. According to R. Fitas and co-workers [1, 2, 12, 13], the absence of physisorbed water greatly affects the charge transfer kinetics. Therefore, this type of water is totally absent within the crystallographic structure of sample C, which explains the very low value of the diffusion coefficient of H^+ within this network and its almost independence of $K(\Lambda, \alpha)$.

The total loss of the electrochemical activity of PbO_2 is due mainly to the absence of OH^- groups, as demonstrated by the differences in the TGA curve in Fig. 2. To better illustrate this behavior of PbO_2 related

Table 2. Equations of I_{peak} as a function of $V^{1/2}$ for the different samples (produced after exposure of the different intermediate oxides to sulfuric acid)

Sample	Equation	Slope, $A/(V\,s^{-1})^{1/2}$
A	$I_{peak} = 1.1547V^{1/2} + 0.0905$	1.15
B	$I_{peak} = 1.573V^{1/2} + 0.1211$	1.57
C	$I_{peak} = 0.280V^{1/2} + 0.0316$	0.28
D	$I_{peak} = 0.718V^{1/2} + 0.0635$	0.72

Table 3. Values of the diffusion coefficient D_{H^+} as a function of the constant $K(\Lambda, \alpha)$

$K(\Lambda,\alpha)$	$D_{H^+} \times 10^{+7}$, $cm^2\,s^{-1}$			
	A	B	C	D
0.6	1.14	2.12	0.07	0.44
0.7	0.84	1.56	0.05	0.33
0.8	0.64	1.19	0.04	0.25
0.9	0.51	0.94	0.03	0.2
1.0	0.41	0.76	0.02	0.16

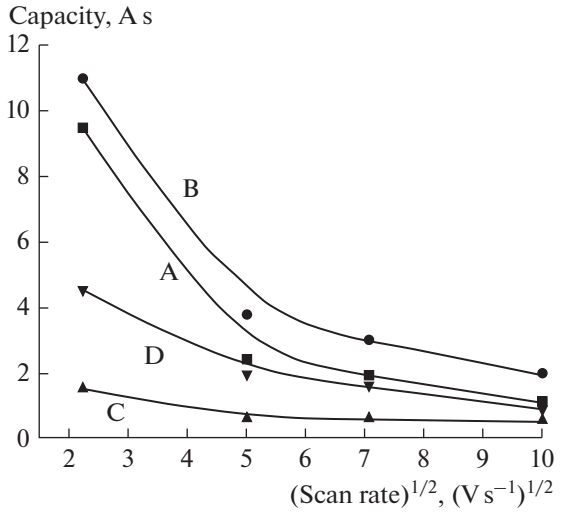

Fig. 8. Effect of scan rate on the capacity of samples A, B, C, and D.

to water, we investigate the influence of the scanning speed on the capacity from the voltammograms of Fig. 5. The capacity is calculated by integrating the area of the voltammogram for each scanning speed used previously (5, 25, 50, and 100 mV/s). The influence of the scanning speed on the capacity of samples A, B, C, and D is shown in Fig. 8. The figure demonstrates clear differences in the capacity values of samples A, B, and D. The capacity is almost independent of the scanning speed for the C sample especially for the high values (difference is greater for sample C at low scanning speeds). Therefore, it can be concluded that the absence of hydroxyl OH^- groups influences largely the capacity of sample C. In addition, the above results lead to that PbO_2 species synthesized from $Pb_{12}O_{19}$ oxide exhibit capacitive performance that is better than PbO_2 of the active mass of the positive plates of the used lead accumulator. In other words, the reduction kinetics is minimal in the case of PbO_2 species of Pb_3O_4 and $Pb_{12}O_{17}$.

As the kinetics represent proton insertion mechanism into PbO_2, this means that the $Pb_{12}O_{19}$ sample has a large amount of structural water in OH^- hydroxyl form. This amount contributes further into the reduction mechanism of PbO_2 produced from $Pb_{12}O_{19}$ compared to PbO_2 of the active mass produced from Pb_3O_4 and $Pb_{12}O_{17}$. Furthermore, the capacity values are maxima for low scanning rate values. This behavior can be explained by the fact that low scanning rate values are better adapted for a solid phase process as shown by the low diffusion coefficient values presented in Fig. 7.

CONCLUSIONS

The study of the different x-ray diffraction (XRD) spectra of lead oxides shows that the intermediate oxides $Pb_{12}O_{19}$, $Pb_{12}O_{17}$, and Pb_3O_4 are unstable. H_2SO_4 was used to transform those intermediate oxides into more stable forms. In particular, $Pb_{12}O_{19}$ has been transformed to PbO_2 after removal of the sulphates. The evaluation of the H^+ proton diffusion coefficient (D_{H^+}) of PbO_2 by voltamperometry has shown that the D_{H^+} of the PbO_2 produced from the $Pb_{12}O_{19}$ oxide is much greater than that of the PbO_2 obtained from battery electrodes.

The high D_{H+} in the structure of PbO_2 allowed the reduction of Pb^{4+} to Pb^{2+}. Since the proton insertion mechanism in PbO_2 represents this reduction kinetics, it indicates that the PbO_2 sample synthesized from the $Pb_{12}O_{19}$ oxide has a large amount of structural water in the OH^- hydroxyl form. This water serves as a proton carrier from the electrolyte, and intervenes during the reduction in the depth of the material. This is a deficiency of Pb^{4+} in the PbO_2 structure which is filled by the protonated species present in the form of hydroxyl groups. This explains the high content of OH^- in the sample of PbO_2 synthesized from the oxide $Pb_{12}O_{19}$ compared to the starting PbO_2.

Hydration of stoichiometric $Pb_{12}O_{19}$ led to lead dioxide which contains structural water. This amount contributed more to the reduction mechanism of PbO_2 produced from $Pb_{12}O_{19}$ than that of the other forms of lead oxides. This was confirmed by the values of the capacity, calculated by integration of the voltammogram area for each scanning speed which showed better than the PbO_2 variety capacitive performance synthesized from $Pb_{12}O_{19}$ oxide. We thus confirm that the proton diffusion is related to the amount of water present in PbO_2, and the recovery of lead dioxide from intermediate oxides is possible. Lead dioxide retrieved from used batteries can be recycled which reduces the risk of its disposal on the underground water.

REFERENCES

1. Fitas, R., Zerroual, L., Chelali, N., and Djellouli, B., Role of hydration water in the reduction process of PbO_2 in lead/acid cells, *J. Power Sources,* 1997, vol. 64, pp. 57–60.
2. Lin Wei, Xuhui Mao, An Lin, and Fuxing Gan, PbO_2–SnO_2 composite anode with interconnected structure for the electrochemical incineration of phenol, *Russ. J. Electrochem.,* 2011, vol. 47, pp. 1394–1398.
3. Brosset, A., *Arkiv. Kemi. Mineral. Band. Geol. A,* 1945, vol. 20, p. 11.
4. Pascal, P., *Nouveau Traité Chimie Minérale,* Paris: Masson, 1960, vol. VIII.
5. Wyckoff, R.W.G., *The Structure of Crystals,* New York: Intersci., 1963, vol. 1.
6. Antonio, P.D. and Santoro, A., Powder neutron diffraction study of chemically prepared β-lead dioxide, *Acta Crystallogr. B,* 1980, vol. 36, p. 2394.

7. Santoro, A., Antonio, P.D., and Caulder, S.M., A neutron powder diffraction study of α- and β-PbO_2 in the positive electrode material of lead-acid batteries, *J. Electrochem. Soc.,* 1983, vol. 13, p. 1451.
8. Gavarri, J.R., Garnier, P., and Boher, P., Proton motions in battery lead dioxides, *J. Solid State Chem.,* 1988, vol. 75, p. 251.
9. Hill, R.J., The crystal structures of lead dioxides from the positive plate of the lead/acid battery, *Mater. Res. Bull.,* 1982, vol. 17, p. 769.
10. Moseley, P.T., Hutchison, J.L., and Bourke, M.A.M., The defect structure of lead dioxide, *J. Electrochem. Soc.,* 1982, vol. 129, p. 876.
11. Fitas, R., Zerroual, L., Chelali, N., and Djellouli, B., Thermal degradation of α- and β-PbO_2 and its relationship to capacity loss, *J. Power Sources,* 2000, vol. 85, p. 56.
12. Fitas, R., Zerroual, L., Chelali, N., and Djellouli, B., Heat treatment of α- and β-battery lead dioxide and its relationship to capacity loss, *J. Power Sources,* 1996, vol. 58, pp. 225–229.
13. Fitas, R., Chelali, N., Zerroual, L., and Djellouli, B., Mechanism of the reduction of α- and β-PbO_2 electrodes using an all-solid-state system, *Solid State Ionics,* 2000, vol. 127, p. 49.
14. Pavlov, D., The lead-acid battery lead dioxide active mass: a gel-crystal system with proton and electron conductivity, *J. Electrochem. Soc.,* 1992, vol. 139, no. 11, p. 3075.
15. Chahmana, N., Matrakova, M., Zerroual, L., and Pavlov, D., Influence of some metal ions on the structure and properties of doped β-PbO_2, *J. Power Sources,* 2009, vol. 191, pp. 51–57.
16. Chahmana, N., Zerroual, L., and Matrakova, M., Physicochemical and electrochemical study of lead acid battery positive active mass (PAM) modified by the addition of bismuth, *Bulgarian Chem. Commun.,* 2016, vol. 48, no. 2, pp. 285–289.
17. Foudia, M., Matracova, M., and Zerroual, L., Effect of a mineral additive on the electrical performances of the positive plate of lead acid battery, *J. Power Sources,* 2015, vol. 279, pp. 146–150.
18. Pavlov, D., Hydration and amorphization of active mass PbO_2 particles and their influence on the electrical properties of the lead-acid battery positive plate, *J. Electrochem. Soc.,* 1989, vol. 136, no. 11, p. 3189.
19. Pohl, J.P. and Shendler, W., The electronic conductivity of compact lead dioxide samples with various stoichiometric compositions, *J. Power Sources,* 1981, vol. 6, p. 245.
20. Foudia, M., Zerroual, L., and Matracova, M., $PbSO_4$ as a precursor for positive active material electrodes, *J. Power Sources,* 2012, vol. 207, pp. 51–55.
21. Noufel, K., Bouzid, A., Chellali, N., and Zerroual, L., Electrochemical performance of γMnO_2 prepared from the active mass of used batteries, *Russ. J. Appl. Chem.,* 2015, vol. 88, no. 10, pp. 1711–1717.
22. Dilmi, O. and Benaicha, M., Electrodeposition and characterization of red selenium thin film-effect of the substrate on the nucleation mechanism, *Russ. J. Electrochem.,* 2017, vol. 53, no. 2, pp. 140–147.
23. Pohl, J.P. and Rickert, H., Elektrochemische Untersuchungen zur Permeation und Löslichkeit von Wasserstoff in Bleidioxid, *J. Phys. Chem.,* 1978, vol. 112, p. 117.
24. Rüetschi, P. and GIovanoli, R., On the presence of OH^- ions, Pb^{2+} ions and cation vacancies in PbO_2, *J. Power Sources,* 1991, vol. 13, p. 81.
25. Rüetschi, P., Influence of crystal structure and interparticle contact on the capacity of PbO_2 electrodes, *J. Electrochem. Soc.,* 1992, vol. 139, no. 5, pp. 1347–1351.
26. Caulder, S.M., Murday, J.S., and Simon, A.C., The hydrogen loss concept of battery failure, the PbO_2 electrode, *J. Electrochem. Soc.,* 1973, vol. 120, p. 1515.
27. Hill, R.J. and Jessel, A.M., The electrochemical activity of PbO_2 a nuclear magnetic resonance study of hydrogen in battery and chemically prepared material, *J. Electrochem. Soc.,* 1987, vol. 134, p. 1326.
28. Samoro, A., D'Amonio, P., and Caulder, S.M., A neutron powder diffraction study of α- and β-PbO_2 in the positive electrode material of lead-acid batteries, *J. Electrochem. Soc.,* 1983, vol. 130, p. 1451.
29. Moseley, P.T., Hutchison, J.L., Wright, C.J., Bourke, M.A.M., Hill, R.I., and Rainey, V.S., Inelastic neutron scattering and transmission electron microscope studies of lead dioxide, *J. Electrochem. Soc.,* 1983, vol. 130, p. 829.
30. Boiler, P., Gamier, P., and Gavarri, J.R., Mise en evidence et localisation des protons dans les bioxydes de plomb PbO_2 α et β chimiques et électrochimiques, *J. Solid-State Chem.,* 1984, vol. 52, p. 146.
31. Gavani, J.R., Gamier, P., Boher, P., Dianoux, A.J., Chedeville, G., and Jacq, B., Proton motions in battery lead dioxides, *J. Solid State Chem.,* 1988, vol. 75, p. 251.
32. Scherrer, P., Bestimmung der inneren Struktur und der Größe von Kolloidteilchen mittels Röntgenstrahlen, *Gttinger Nachrichten,* 1918, vol. 2, p. 98.
33. Matsuda, H. and Ayabe, Y., The theory of the cathode-ray polarography of Randles-Sevcik, *Z. Elektrochim. Angew. Phys. Chem.,* 1955, vol. 59, pp. 494–503.
34. Münzberg, R. and Pohl, J.P., *Proc. 15th Int. Power Sources Symp.,* Brighton, 1986.
35. Chelali, N. and Guitton, J., Electrochemical behavior of α- and β-PbO_2. Part I: proton diffusion from "all solid-state" protonic electrolyte, *Solid State Ionics,* 1994, vol. 73, p. 227.

SPELL: 1. ok